ASTRONOMY & ASTROPHYSICS
SUPPLEMENT SERIES

Astron. Astrophys. Suppl. Ser. **142**, 317–323 (2000)

Electron-impact excitation of Fe^{7+}

D.C. Griffin[1], **M.S. Pindzola**[2], **and N.R. Badnell**[3]

[1] Department of Physics, Rollins College, Winter Park, FL 32789, U.S.A.
[2] Department of Physics, Auburn University, Auburn, AL 36849, U.S.A.
[3] Department of Physics and Applied Physics, University of Strathclyde, Glasgow G4 ONG, UK

Received September 20; accepted December 22, 1999

Abstract. Electron-impact excitation cross sections for Fe^{7+} are calculated using R-matrix close-coupling theory. The calculation includes 33 LS terms of the seven configurations: 3p^{6}3d, 3p^{5}3d^2, 3p^{5}3d4s, 3p^{6}4s, 3p^{6}4p, 3p^{6}4d, and 3p^{6}4f. Following an intermediate-coupling frame transformation of the LS K-matrices, cross sections and effective collision strengths are obtained for 2926 transitions among 77 LSJ levels of the original seven configurations. After the solution of the corresponding collisional-radiative equations, the emission line ratio involving a blend of the 3p^{6}4f ^{2}F $\rightarrow$ 3p^{6}3d ^{2}D transitions at around 131 A and another blend of the 3p^{5}3d^2 ^{2}P $\rightarrow$ 3p^{6}3d ^{2}D and 3p^{5}3d^2 ^{2}D $\rightarrow$ 3p^{6}3d ^{2}D transitions at around 168 A is found to provide a very useful electron-temperature diagnostic.

Key words: atomic data — Sun: corona

1. Introduction

Collisional data for members of the Fe isonuclear sequence are important for the interpretation of astrophysical plasmas associated with the solar corona, nebulae, and stellar atmospheres (Butler et al. 1998). As the field of X-ray astronomy continues to blossom with the increased availability of high-resolution satellite observatories, emission lines from the more highly charged Fe atomic ions will be recorded in increasingly greater detail. In this paper, we apply R-matrix scattering theory to the calculation of electron-impact excitation cross sections for Fe^{7+}. Previous distorted-wave and close-coupling calculations for Fe^{7+} (Pindzola et al. 1988) included only a small number of configurations and did not attempt to map out the sometimes rich resonance structure found near excitation thresholds. The calculation reported below includes 33 LS terms of the seven configurations: 3p^{6}3d, 3p^{5}3d^2, 3p^{5}3d4s, 3p^{6}4s, 3p^{6}4p, 3p^{6}4d, and 3p^{6}4f. Employing a recently developed intermediate-coupling frame transformation (ICFT) (Griffin et al. 1998) of the K-matrices calculated from an LS R-matrix calculation, cross sections and Maxwellian-averaged effective collision strengths are obtained for 2926 transitions among the 77 LSJ levels of the original seven configurations.

In addition to the collisional data for Fe^{7+}, we have determined dipole-allowed radiative rates between the 5 even parity levels and the 72 odd parity levels. The entire set of atomic data for Fe^{7+}, including the effective collision strengths and radiative rates, is put in a general format for easy interface with plasma modeling codes. The formatted data set is now available via the Oak Ridge National Laboratory (ORNL) Controlled Fusion Atomic Data Center internet site (http://www.cfadc.ornl.gov). As way of example, we used the ADAS collisional-radiative modeling codes (Summers 1994) and the Fe^{7+} atomic data set to calculate an emission line ratio involving a blend of the 3p^{6}4f ^{2}F $\rightarrow$ 3p^{6}3d ^{2}D transitions at around 131 A and another blend of the 3p^{5}3d^2 ^{2}P $\rightarrow$ 3p^{6}3d ^{2}D and 3p^{5}3d^2 ^{2}D $\rightarrow$ 3p^{6}3d ^{2}D transitions at around 168 A. This particular line ratio provides a very useful electron temperature diagnostic for a wide range of electron densities.

The remainder of this paper is organized as follows: in Sect. 2 we present our atomic structure and R-matrix scattering calculations for Fe^{7+}, in Sect. 3 we present our ADAS line emission ratio calculation for Fe^{7+}, and in Sect. 4 we summarize our findings.

2. Atomic structure and scattering calculations

2.1. Bound-state calculations

The bound-state radial wavefunctions for Fe^{7+} were calculated using Froese Fischer's Hartree-Fock program (Froese Fischer 1991). The 1s, 2s, 2p, 3s, 3p, and 3d orbitals were generated from a configuration-average Hartree-Fock (CAHF) calculation on the 3p^{5}3d^2 configuration, while

---

Send offprint requests to: D.C. Griffin the 4s orbital was generated from a frozen-core CAHF calculation on $3p^53d4s$ configuration. Finally the 4p, 4d, and 4f orbitals were generated from frozen-core CAHF calculations on the $3p^64p$, $3p^64d$, and $3p^64f$ configurations, respectively. These orbitals were then employed within Breit-Pauli configuration-interaction (CI) calculations on the 5 even levels arising from the configurations $3p^63d$, $3p^64s$, and $3p^64d$, and the 72 odd levels arising from the configurations $3p^53d^2$, $3p^53d4s$, $3p^64p$, and $3p^64f$.

In Table 1, we present the energies resulting from these CI calculations in comparison to available experimental data. The LS designations should be considered as labels only; for many of these levels, there is strong mixing due to the electrostatic interactions between LS terms with different parents, the spin-orbit interactions, and the interactions between configurations. For example, level 50 labeled as $3p^53d^2(^3F)^2D_{3/2}$ in Table 1 is actually: $0.845 \times 3p^53d^2(^3F)^2D_{3/2} + 0.418 \times 3p^53d^2(^1D)^2D_{3/2} + 0.329 \times 3p^53d^2(^3P)^2D_{3/2}$ plus some smaller eigenvector components; this amount of mixing between different LS parents is typical of many of the levels of the $3p^53d^2$ configuration.

We see that the agreement between experiment and theory is quite good for those few lower levels of the $3p^53d^2$ configuration for which experimental measurements exist; however, the differences grow to an average of 3.2 eV for the 6 highest levels of this configuration, all of which are important because of their strong radiative rates to the ground-state configuration. On the other hand, the average differences between experiment and theory for the levels of $3p^64p$, $3p^64f$, and $3p^53d4s$ are only 1.11 eV, 1.64 eV, and 1.49 eV, respectively. In order to account for ground-state correlation, it would have been necessary to include such configurations as $3s^03p^63d^3$, $3s3p^63d^2$, and $3s^23p^43d^3$ in our configuration-interaction expansion of the target; but then, in order to account for final-state correlation, one should also include the configurations formed from single and double promotions from the 3s subshell to the 3d subshell and double promotions from the 3p subshell to the 3d subshell for all excited configurations, and that would have made the problem prohibitively large. Finally, if the levels of $3s^23p^65\ell$ and $3s3p^63d^2$ (which are in the same energy range as some of the upper levels in our present calculation) had been included in our close-coupling expansion of the target, they would have some effect on our scattering calculations to the more highly excited states through both coupling, which would have tended to decrease the cross sections, and resonance contributions, which would have enhanced the cross sections. However, to include these configurations in our close-coupling expansion would have added 10 LS terms and 25 levels to an already large calculation.

In order to provide the radiative data necessary to do collisional-radiative modeling for Fe^{7+}, we have calculated all dipole-allowed radiative rates between the 5 even levels and the 72 odd levels listed in Table 1. Of particular importance are the strong radiative rates from the highest 6 levels of the $3p^53d^2$ configuration and the two levels of the $3p^64f$ configuration to the $3p^63d$ ground-state configuration. These transitions occur in the far vacuum UV, have been observed using existing satellites, and should be accessible, under higher resolution, with the low-energy transmission grating of the recently launched Chandra X-ray satellite observatory (Brickhouse 1999). These particular radiative rates should be most strongly affected by configuration interaction with configurations formed from double electron promotions from the 3p subshell to the 3d subshell. For that reason, we have performed an expanded CI calculation of these radiative rates in which we also included those levels of the $3p^43d^3$ configuration that mix strongly with the levels of $3p^63d$, those levels of the $3p^33d^4$ that mix strongly with the 6 highest levels of the $3p^53d^2$ configuration, and those levels of the $3p^43d^24f$ configuration that mix strongly with the levels of the $3p^64f$ configuration.

In Table 2, we compare the radiative rates that result from the two CI calculations for these particular transitions. For both calculations, we adjusted the energies to the experimental values before calculating the rates. As can be seen, this extra CI reduces the radiative rates for the transitions from the 6 highest levels of the $3p^53d^2$ configuration by an average of 21%. On the other hand, the radiative rates for the transitions from the $3p^64f$ configuration are reduced by less than 10%.

2.2. Excitation calculations

Our collisional excitation calculations were performed using the intermediate-coupling frame transformation (ICFT) method, which is described in detail in Griffin et al. (1998). It is based on the application of multichannel quantum defect theory, in which unphysical K-matrices are first generated from an R-matrix close-coupling calculation in pure LS coupling and are then transformed to intermediate coupling. The physical K matrices are then determined from a simple frame transformation. This method has been shown (Griffin et al. 1998 and Griffin et al. 1999a) to eliminate many of the problems associated with the transformation of the physical LS S- or K-matrices to intermediate coupling and is capable of producing accurate level-to-level cross sections in far less time than required for a full Breit-Pauli R-matrix calculation.

In the present case, we first performed an LS R-matrix calculation with exchange, which included all 33 terms arising from the $3p^63d$, $3p^53d^2$, $3p^53d4s$, $3p^64s$, $3p^64p$, $3p^64d$, and $3p^64f$ configurations in the close-coupling expansion and all $LS\Pi$ partial waves from $L = 0$ to 14. This allowed us to use our ICFT transformation method to generate the contributions between the 77 levels listed in Table 1 for the $J\Pi$ partial waves from $J = 0$ to 12. However, this partial-wave expansion must be extended to

Table 1. Energies in eV (relative to $3p^63d\ ^2D_{3/2}$) of the levels in the 33-term, 77-level R-matrix calculation on Fe^{7+}

Index	Level	Theor. Energy	Exp. Energy[a]	Index	Level	Theor. Energy	Exp. Energy[a]
1	$3p^63d\ ^2D_{3/2}$	0.00	0.00	2	$3p^63d\ ^2D_{5/2}$	0.24	0.23
3	$3p^53d^2(^3F)^4D_{1/2}$	47.75	—	4	$3p^53d^2(^3F)^4D_{3/2}$	47.86	—
5	$3p^53d^2(^3F)^4D_{5/2}$	48.05	—	6	$3p^53d^2(^3F)^4D_{7/2}$	48.34	—
7	$3p^53d^2(^3F)^4G_{11/2}$	50.62	—	8	$3p^53d^2(^3F)^4G_{9/2}$	50.82	—
9	$3p^53d^2(^3F)^4G_{7/2}$	51.07	—	10	$3p^53d^2(^3P)^4P_{5/2}$	51.20	—
11	$3p^53d^2(^3F)^4G_{5/2}$	51.34	—	12	$3p^53d^2(^3P)^4P_{3/2}$	51.57	—
13	$3p^53d^2(^3P)^4P_{1/2}$	51.85	—	14	$3p^53d^2(^3F)^4F_{3/2}$	52.57	—
15	$3p^53d^2(^3F)^4F_{5/2}$	52.73	—	16	$3p^53d^2(^3F)^4F_{9/2}$	52.80	—
17	$3p^53d^2(^3F)^4F_{7/2}$	52.91	—	18	$3p^53d^2(^1D)^2D_{5/2}$	53.34	—
19	$3p^53d^2(^1G)^2F_{5/2}$	53.43	53.47	20	$3p^53d^2(^1D)^2D_{3/2}$	53.56	—
21	$3p^64s\ ^2S_{1/2}$	53.75	—	22	$3p^53d^2(^1G)^2F_{7/2}$	53.88	53.88
23	$3p^53d^2(^1D)^2P_{1/2}$	54.60	—	24	$3p^53d^2(^1D)^2P_{3/2}$	55.27	—
25	$3p^53d^2(^1G)^2H_{11/2}$	55.35	—	26	$3p^53d^2(^1D)^2F_{7/2}$	55.62	55.50
27	$3p^53d^2(^3F)^2G_{7/2}$	55.95	—	28	$3p^53d^2(^3F)^2G_{9/2}$	56.30	—
29	$3p^53d^2(^1G)^2H_{9/2}$	56.60	—	30	$3p^53d^2(^1D)^2F_{5/2}$	57.09	56.95
31	$3p^53d^2(^3P)^4D_{7/2}$	57.24	—	32	$3p^53d^2(^3P)^4D_{5/2}$	57.41	—
33	$3p^53d^2(^3P)^4D_{3/2}$	57.65	—	34	$3p^53d^2(^3P)^4D_{1/2}$	57.88	—
35	$3p^53d^2(^3P)^2D_{3/2}$	59.99	—	36	$3p^53d^2(^3P)^2D_{5/2}$	60.48	—
37	$3p^53d^2(^3P)^4S_{3/2}$	60.80	—	38	$3p^53d^2(^3P)^2S_{1/2}$	60.80	—
39	$3p^53d^2(^1G)^2G_{9/2}$	61.19	—	40	$3p^53d^2(^1G)^2G_{7/2}$	61.28	—
41	$3p^53d^2(^1S)^2P_{3/2}$	64.14	63.05	42	$3p^64p\ ^2P_{1/2}$	64.28	63.27
43	$3p^64p\ ^2P_{3/2}$	65.02	63.92	44	$3p^53d^2(^1S)^2P_{1/2}$	65.69	64.57
45	$3p^53d^2(^3F)^2F_{5/2}$	69.17	66.44	46	$3p^53d^2(^3F)^2F_{7/2}$	69.86	67.17
47	$3p^53d^2(^3P)^2P_{1/2}$	76.33	73.39	48	$3p^53d^2(^3P)^2P_{3/2}$	76.70	73.79
49	$3p^53d^2(^3F)^2D_{5/2}$	77.86	73.95	50	$3p^53d^2(^3F)^2D_{3/2}$	77.88	74.03
51	$3p^64d\ ^2D_{3/2}$	82.72	—	52	$3p^64d\ ^2D_{5/2}$	82.77	—
53	$3p^64f\ ^2F_{5/2}$	96.33	94.69	54	$3p^64f\ ^2F_{7/2}$	96.34	94.70
55	$3p^53d(^3P)4s\ ^4P_{1/2}$	103.49	—	56	$3p^53d(^3P)4s\ ^4P_{3/2}$	103.79	—
57	$3p^53d(^3P)4s\ ^4P_{5/2}$	104.35	—	58	$3p^53d(^3P)4s\ ^2P_{1/2}$	105.14	103.86
59	$3p^53d(^3P)4s\ ^2P_{3/2}$	105.78	104.50	60	$3p^53d(^3F)4s\ ^4F_{9/2}$	105.84	—
61	$3p^53d(^3F)4s\ ^4F_{7/2}$	106.15	105.03	62	$3p^53d(^3F)4s\ ^4F_{5/2}$	106.48	105.37
63	$3p^53d(^3F)4s\ ^4F_{3/2}$	106.81	105.74	64	$3p^53d(^3F)4s\ ^2F_{7/2}$	107.36	106.00
65	$3p^53d(^3F)4s\ ^2F_{5/2}$	108.03	106.70	66	$3p^53d(^3D)4s\ ^4D_{7/2}$	110.02	108.45
67	$3p^53d(^3D)4s\ ^4D_{5/2}$	110.26	108.70	68	$3p^53d(^3D)4s\ ^4D_{3/2}$	110.38	108.79
69	$3p^53d(^3D)4s\ ^4D_{1/2}$	110.47	108.89	70	$3p^53d(^1D)4s\ ^2D_{5/2}$	110.75	108.98
71	$3p^53d(^1D)4s\ ^2D_{3/2}$	110.99	109.27	72	$3p^53d(^1F)4s\ ^2F_{5/2}$	111.22	109.64
73	$3p^53d(^1F)4s\ ^2F_{7/2}$	111.49	110.01	74	$3p^53d(^3D)4s\ ^2D_{3/2}$	111.94	110.24
75	$3p^53d(^3D)4s\ ^2D_{5/2}$	112.07	110.45	76	$3p^53d(^1P)4s\ ^2P_{3/2}$	129.51	—
77	$3p^53d(^1P)4s\ ^2P_{1/2}$	129.51	—				

[a] Sugar & Corliss (1985).

much higher values of J in order to provide accurate data for collisional-radiative modeling calculations. Therefore, we also performed a no-exchange LS R-matrix calculation for all LSΠ partial waves from $L = 11$ to 50; this allowed us to generate intermediate-coupling results for all JΠ partial waves from $J = 13$ to 48. These high J contributions were then topped-up for the dipole-allowed transitions using a method originally described by Burgess 1974 for LS coupling and implemented in our ICFT program for intermediate coupling; additionally, the non-dipole transitions were topped-up assuming a geometric series in J.

For all our calculations, the size of the R-matrix box was set to 8.02 a.u., 27 basis orbitals were used to represent the continuum orbitals for each value of the angular momentum; this was more than sufficient to allow us to carry out our calculations to a maximum energy of 600 eV. The long-range multipole contributions were included in the asymptotic region. For the asymptotic part of the calculation, we found that an energy mesh with a separation between adjacent energy points of 0.0165 eV allowed us to resolve the vast majority of narrow resonances in the energy range up through the highest threshold.

Table 2. Dipole radiative rates from the six highest levels of the $3p^53d^2$ configuration and the two levels of the $3p^64f$ configuration to the two levels of the $3p^63d$ ground-state configuration

Transition	$A_r(s^{-1})^a$	$A_r(s^{-1})^b$	Ratio^c
$3p^53d^2(^3F)^2F_{5/2} \rightarrow 3p^63d\ ^2D_{3/2}$	$1.32\,10^{11}$	$0.98\,10^{11}$	0.742
$3p^53d^2(^3F)^2F_{5/2} \rightarrow 3p^63d\ ^2D_{5/2}$	$6.68\,10^{9}$	$4.49\,10^{9}$	0.672
$3p^53d^2(^3F)^2F_{7/2} \rightarrow 3p^63d\ ^2D_{5/2}$	$1.42\,10^{11}$	$1.04\,10^{11}$	0.732
$3p^53d^2(^3P)^2P_{1/2} \rightarrow 3p^63d\ ^2D_{3/2}$	$2.79\,10^{11}$	$2.27\,10^{11}$	0.814
$3p^53d^2(^3P)^2P_{3/2} \rightarrow 3p^63d\ ^2D_{3/2}$	$2.81\,10^{10}$	$2.50\,10^{10}$	0.890
$3p^53d^2(^3P)^2P_{3/2} \rightarrow 3p^63d\ ^2D_{5/2}$	$2.53\,10^{11}$	$2.05\,10^{11}$	0.810
$3p^53d^2(^3F)^2D_{5/2} \rightarrow 3p^63d\ ^2D_{3/2}$	$2.25\,10^{10}$	$1.67\,10^{10}$	0.742
$3p^53d^2(^3F)^2D_{5/2} \rightarrow 3p^63d\ ^2D_{5/2}$	$3.59\,10^{11}$	$3.05\,10^{11}$	0.850
$3p^53d^2(^3F)^2D_{3/2} \rightarrow 3p^63d\ ^2D_{3/2}$	$3.48\,10^{11}$	$2.93\,10^{11}$	0.842
$3p^53d^2(^3F)^2D_{3/2} \rightarrow 3p^63d\ ^2D_{5/2}$	$3.78\,10^{10}$	$3.12\,10^{10}$	0.825
$3p^64f\ ^2F_{5/2} \rightarrow 3p^63d\ ^2D_{3/2}$	$1.81\,10^{11}$	$1.64\,10^{11}$	0.906
$3p^64f\ ^2F_{5/2} \rightarrow 3p^63d\ ^2D_{5/2}$	$1.32\,10^{10}$	$1.19\,10^{10}$	0.902
$3p^64f\ ^2F_{7/2} \rightarrow 3p^63d\ ^2D_{5/2}$	$1.96\,10^{11}$	$1.78\ 10^{11}$	0.908

[a] Calculated from CI calculations involving the 77 levels listed in Table 1, with the energies adjusted to the experimental values.

[b] Calculated from CI calculations involving the 77 levels listed in Table 1 plus configuration-interaction with the levels of $3p^43d^3$ that mix strongly with $3p^63d$, the levels of $3p^33d^4$ that mix strongly with $3p^53d^2$, and the levels of $3p^43d^24f$ that mix strongly with the levels of $3p^64f$. Again, the energies were adjusted to the experimental values.

[c] The ratio of the rates calculated with the extra CI to the rates calculated without it.

In Figs. 1, 2, 3, and 4, we show our calculated cross section from the two levels of $3p^63d$ to the highest six levels of the $3p^53d^2$ configuration and to the two levels of the $3p^64f$ configuration. As can be seen, the non-dipole allowed transitions $3p^63d\ ^2D_{3/2} \rightarrow 3p^53d^2(^3F)^2F_{7/2}$ and $3p^63d\ ^2D_{5/2} \rightarrow 3p^53d^2(^3P)^2P_{1/2}$ are dominated by resonance contributions in the low-energy region. In addition, resonant contributions are important in the low-energy region for the dipole-allowed transitions $3p^63d\ ^2D_{3/2} \rightarrow 3p^53d^2(^3F)^2F_{5/2}$, $3p^63d\ ^2D_{5/2} \rightarrow 3p^53d^2(^3F)^2F_{5/2}$, and $3p^63d\ ^2D_{5/2} \rightarrow 3p^53d^2(^3F)^2F_{7/2}$, but are of less importance for the other transitions shown.

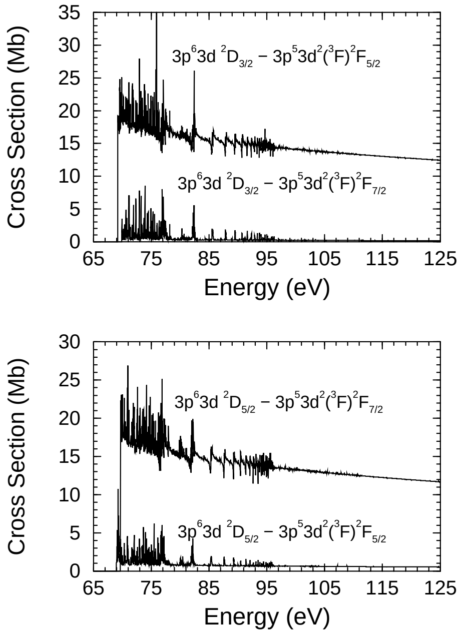

Fig. 1. Electron-impact excitation cross sections for transitions from the levels of $3p^63d\ ^2D$ to the levels of $3p^53d^2(^3F)^2F$ in Fe^{7+}

As discussed in the last subsection, the effects of configuration interaction with configurations formed from double electron promotions from the 3p subshell to the 3d subshell reduce the radiative rates for transitions from these same levels of the $3p^53d^2$ configuration to the ground-state configuration by approximately 20% and the transitions from the levels of $3p^64f$ to the levels of the ground-state configuration by about 10%. If we had been able to include these correlations in our scattering calculations, they would have also reduced the cross sections for the strong-dipole allowed transitions from the ground state to these levels. Furthermore, as we have already mentioned, coupling to more highly excited bound states would affect these cross sections, especially those for the excitations to the $3p^64f$ levels. Finally, it has been shown from extensive pseudo-state calculations (see for example, Bartschat & Bray 1997; Marchalant et al. 1997, and Griffin et al. 1999b) that coupling between the bound states and the target continuum will tend to further reduce the excitation cross sections, and should be more important for excitations to the $3p^64f$ levels than for the excitations to the levels of $3p^53d^2$; however, these effects should be less than 20% for a seven-times ionized species (Griffin et al. 1999b). Thus, we might expect that our calculated cross sections for the strong dipole-allowed excitations to these levels to be uncertain at the 20% to 30% level, and that in general, our calculations will tend to overestimate these cross sections. The accuracy of the non-dipole transitions, that are often dominated by resonances at lower energies, is much more difficult to estimate.

For collisional-radiative modeling calculations, we require rate coefficients, rather than cross sections. However, the effective collision strength, first introduced by Seaton (Seaton 1953), is much more convenient for input to such calculations because it has a much more gradual variation with the electron temperature than the rate coefficient. It is defined by the equation:

$$\Upsilon_{ij} = \int_0^{\infty} \Omega(i \rightarrow j) \exp\left(\frac{-\epsilon_j}{kT_e}\right) \mathrm{d}\left(\frac{\epsilon_j}{kT_e}\right), \qquad (1)$$

where Ω_{ij} is the collision strength for the transition from level i to level j and ϵ_j is the continuum energy of the final scattered electron. The rate coefficients for collisional

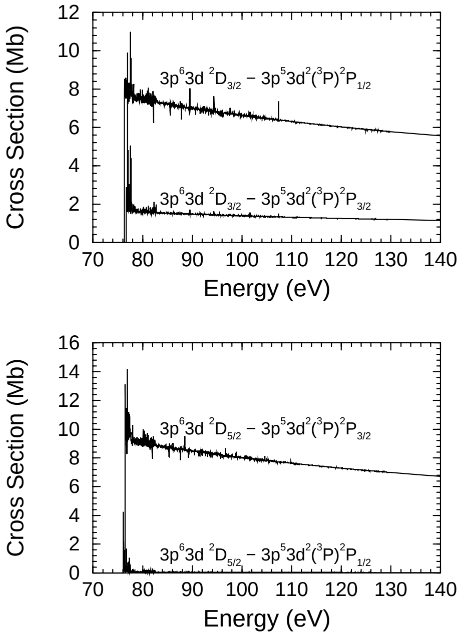

Fig. 2. Electron-impact excitation cross sections for transitions from the levels of $3p^63d\ ^2D$ to the levels of $3p^53d^2(^3P)^2P$ in Fe^{7+}

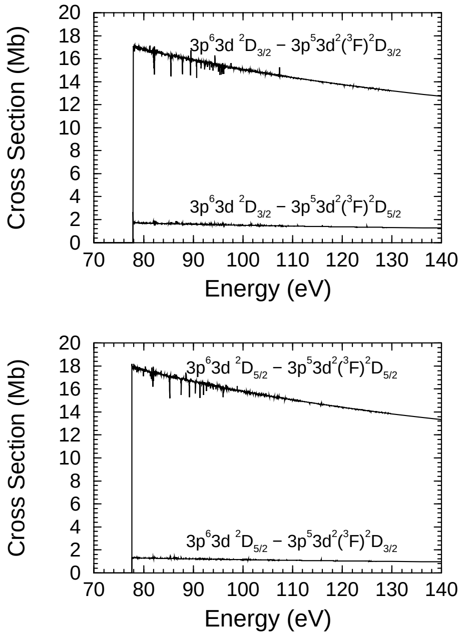

Fig. 3. Electron-impact excitation cross sections for transitions from the levels of $3p^63d\ ^2D$ to the levels of $3p^53d^2(^3F)^2D$ in Fe^{7+}

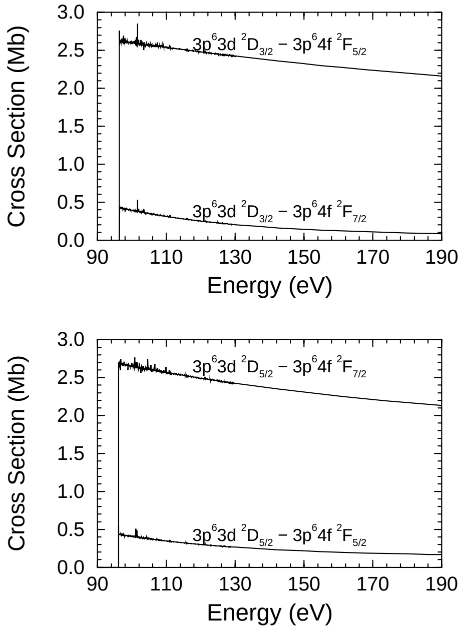

Fig. 4. Electron-impact excitation cross sections for transitions from the levels of $3p^63d\ ^2D$ to the levels of $3p^64f\ ^2F$ in Fe^{7+}

excitation $q_{i\to j}$ and de-excitation $q_{j\to i}$ can then be determined from the equations

$$q_{i\to j} = \frac{2\sqrt{\pi}\alpha c a_0^2}{\omega_i}\sqrt{\frac{I_{\rm H}}{kT_{\rm e}}}\exp\left(-\frac{\Delta E_{ij}}{kT_{\rm e}}\right)\Upsilon_{ij}, \tag{2}$$

and

$$q_{j\to i} = \frac{\omega_i}{\omega_j}\exp\left(\frac{\Delta E_{ij}}{kT_{\rm e}}\right)q_{i\to j}, \tag{3}$$

where $2\sqrt{\pi}\alpha c a_0^2 = 2.1716\ 10^{-8}$ cm^3 s^{-1}, $I_{\rm H} = 13.6058$ eV, ΔE_{ij} is the threshold energy for the transition from level i to level j, and ω_i and ω_j are the statistical weights of level i and level j, respectively.

Our table of collision strengths for the 2926 transitions among the 77 LSJ levels listed in Table 1 is far too large to be shown here. However, in Table 3, we show the effective collision strengths for the same transitions for which we presented cross sections in Figs. 1, 2, 3, and 4. It is the transitions to the four highest levels of the $3p^53d^2$ configuration and the two levels of the $3p^64f$ configuration that are of primary importance for the line-emission intensity ratios discussed in the next section.

3. ADAS line emission calculations

The atomic data set for Fe^{7+}, which is now available at the ORNL internet site, contains angular momentum quantum numbers and energies for each of the 77 LSJ levels, followed by radiative rates and effective collision strengths for all 2926 possible transitions among pairs of levels. The energies were adjusted to the experimental values, where known, and the radiative rates for those transitions shown in Table 2 were those determined from our extended CI calculation. Although specific for ADAS, the general format should allow easy interface with most plasma modeling codes.

By way of example, we used the ADAS collisional-radiative modeling codes and the Fe^{7+} atomic data set to calculate equilibrium populations for all 77 LSJ levels over a range of electron temperatures and densities. Specific spectral intensities were then used to construct an

Table 3. Effective collision strengths from the two levels of the $3p^63d$ ground-state configuration to the six highest levels of the $3p^53d^2$ configuration and the two levels of the $3p^64f$ configuration

	Electron temperature (K)					
Transition	6.40 10^4	1.28 10^5	3.20 10^5	6.40 10^5	1.28 10^6	3.20 10^6
$3p^63d\ ^2D_{3/2} \rightarrow 3p^53d^2(^3F)^2F_{5/2}$	4.44	4.47	4.62	4.99	5.72	7.24
$3p^63d\ ^2D_{3/2} \rightarrow 3p^53d^2(^3F)^2F_{7/2}$	0.268	0.215	0.143	0.100	0.069	0.042
$3p^63d\ ^2D_{3/2} \rightarrow 3p^53d^2(^3P)^2P_{1/2}$	2.04	2.08	2.18	2.39	2.77	3.55
$3p^63d\ ^2D_{3/2} \rightarrow 3p^53d^2(^3P)^2P_{3/2}$	0.454	0.451	0.462	0.498	0.571	0.721
$3p^63d\ ^2D_{3/2} \rightarrow 3p^53d^2(^3F)^2D_{5/2}$	0.464	0.475	0.500	0.546	0.634	0.810
$3p^63d\ ^2D_{3/2} \rightarrow 3p^53d^2(^3F)^2D_{3/2}$	4.59	4.71	4.98	5.49	6.41	8.26
$3p^63d\ ^2D_{3/2} \rightarrow 3p^64f\ ^2F_{5/2}$	0.878	0.892	0.954	1.10	1.35	1.89
$3p^63d\ ^2D_{3/2} \rightarrow 3p^64f\ ^2F_{7/2}$	0.128	0.118	0.097	0.087	0.066	0.051
$3p^63d\ ^2D_{5/2} \rightarrow 3p^53d^2(^3F)^2F_{5/2}$	0.567	0.488	0.404	0.371	0.374	0.422
$3p^63d\ ^2D_{5/2} \rightarrow 3p^53d^2(^3F)^2F_{7/2}$	6.35	6.36	6.55	7.05	8.06	10.2
$3p^63d\ ^2D_{5/2} \rightarrow 3p^53d^2(^3P)^2P_{1/2}$	0.055	0.039	0.026	0.021	0.017	0.014
$3p^63d\ ^2D_{5/2} \rightarrow 3p^53d^2(^3P)^2P_{3/2}$	3.71	3.78	3.97	4.34	5.03	6.42
$3p^63d\ ^2D_{5/2} \rightarrow 3p^53d^2(^3F)^2D_{5/2}$	7.19	7.39	7.82	8.61	10.1	13.0
$3p^63d\ ^2D_{5/2} \rightarrow 3p^53d^2(^3F)^2D_{3/2}$	0.525	0.538	0.565	0.619	0.718	0.918
$3p^63d\ ^2D_{5/2} \rightarrow 3p^64f\ ^2F_{5/2}$	0.202	0.193	0.175	0.168	0.171	0.194
$3p^63d\ ^2D_{5/2} \rightarrow 3p^64f\ ^2F_{7/2}$	1.34	1.36	1.44	1.64	2.01	2.78

emission line ratio involving a blend of the $3p^64f\ ^2F \rightarrow 3p^63d\ ^2D$ transitions at around 131 A and another blend of the $3p^53d^2(^3P)\ ^2P \rightarrow 3p^63d\ ^2D$ and $3p^53d^2(^3F)\ ^2D \rightarrow 3p^63d\ ^2D$ transitions at around 168 A. The first blend contains the transitions $3p^64f\ ^2F_{\frac{5}{2}} \rightarrow 3p^63d\ ^2D_{\frac{3}{2}}$ at 130.9 A, $3p^64f\ ^2F_{\frac{5}{2}} \rightarrow 3p^63d\ ^2D_{\frac{5}{2}}$ at 131.3 A, and $3p^64f\ ^2F_{\frac{7}{2}} \rightarrow 3p^63d\ ^2D_{\frac{5}{2}}$ at 131.2 A. The second blend contains the transitions $3p^53d^2(^3P)^2P_{\frac{1}{2}} \rightarrow 3p^63d\ ^2D_{\frac{3}{2}}$ at 168.9 A, $3p^53d^2(^3P)^2P_{\frac{3}{2}} \rightarrow 3p^63d\ ^2D_{\frac{3}{2}}$ at 168.0 A, $3p^53d^2(^3F)^2D_{\frac{5}{2}} \rightarrow 3p^63d\ ^2D_{\frac{3}{2}}$ at 167.7 A, $3p^53d^2(^3F)^2D_{\frac{3}{2}} \rightarrow 3p^63d\ ^2D_{\frac{3}{2}}$ at 167.5 A, $3p^53d^2(^3P)^2P_{\frac{3}{2}} \rightarrow 3p^63d\ ^2D_{\frac{5}{2}}$ at 168.5 A, $3p^53d^2(^3F)^2D_{\frac{5}{2}} \rightarrow 3p^63d\ ^2D_{\frac{5}{2}}$ at 168.2 A, and $3p^53d^2(^3F)^2D_{\frac{3}{2}} \rightarrow 3p^63d\ ^2D_{\frac{5}{2}}$ at 168.0 A.

The emission line ratio as a function of electron temperature at an electron density of 1.0 10^8 cm^{-3} is shown in Fig. 5. This line ratio provides a very useful electron temperature diagnostic; however, since it involves only strong dipole-allowed transitions, it is found to be very insensitive to changes in the electron density. With the Fe^{7+} atomic data set and the observed spectrum in hand, other choices for line emission ratios may be quickly chosen and processed to provide further plasma temperature and density information. Furthermore, with the low-energy grating on the Chandra X-ray satellite observatory, it should be possible to resolve many of the components that constitute these two blended lines and, in combination with this data set, could provide a much more complete set of diagnostics.

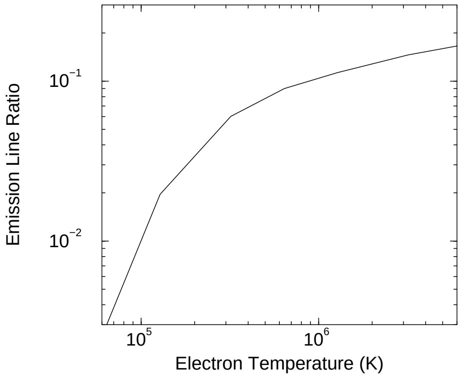

Fig. 5. Emission line ratio for a blend of the $3p^64f\ ^2F \rightarrow 3p^63d\ ^2D$ transitions at a wavelength of about 131 A divided by a blend of the $3p^53d^2(^3P)^2P \rightarrow 3p^63d\ ^2D$ and $3p^53d^2(^3F)^2D \rightarrow 3p^63d\ ^2D$ transitions at a wavelength of about 168 A

4. Summary

Electron-impact excitation cross sections and Maxwellian-averaged effective collision strengths were determined for Fe^{7+} using R-matrix close-coupling theory in conjunction with multi-channel quantum defect theory and the intermediate-coupling frame transformation method. Effective collision strengths were determined for all 2926 transitions among the 77 levels of seven ground and low-lying excited configurations. Furthermore, radiative rates were determined for all dipole-allowed transitions from Breit-Pauli configuration-interaction calculations; these rates, in combination with energies and effective collision strengths, were used to construct a collisional-radiative atomic data set for Fe^{7+}, which is now available at the ORNL Controlled Fusion Atomic Data Center internet site. The ADAS collisional-radiative modeling codes and the Fe^{7+} atomic data set were used to calculate equilibrium populations for all 77 LSJ levels over a range of electron temperatures and densities. Spectral intensities for ten dipole-allowed transitions in Fe^{7+} were then calculated to produce a single blended line ratio that provides a very useful electron temperature diagnostic.

Acknowledgements. This work was supported by the U.S. Department of Energy under Contract Nos. DE-FG02-96-ER54367 with Rollins College and DE-FG05-96ER54348 with Auburn University and by the U.K. Particle Physics and Astronomy Research Council under Grant No. PPA/G/S/1997/00783 with the University of Strathclyde.

References

Bartschat K., Bray I., 1997, J. Phys. B 30, L109
Brickhouse N., 1999 (private communication)
Burgess A., 1974, J. Phys. B 7, L364
Butler K., 1998, in "Atomic and Molecular Data and Their Applications", AIP Conf. Proc. 434, 23
Froese Fischer C., 1991, Comput. Phys. Commun. 64, 369
Griffin D.C., Badnell N.R., Pindzola M.S., 1998, J. Phys. B 31, 3713
Griffin D.C., Badnell N.R., Pindzola M.S., Shaw J.A., 1999a, J. Phys. B 32, 2139
Griffin D.C., Badnell N.R., Pindzola M.S., 1999b (submitted to J. Phys. B)
Marchalant P.J., Bartschat K., Bray I., 1997, J. Phys. B 30, L435
Pindzola M.S., Griffin D.C., Bottcher C., 1988, Phys. Rev. A 39, 2385
Seaton M.J., 1953, J. Proc. R. Soc. A 218, 2111
Sugar J., Corliss C., 1985, J. Phys. Chem. Ref. Data 14, No. 2
Summers H.P., 1994, "Atomic Data and Analysis Structure (ADAS) User Manual", JET-IR 06